Subharmonic frequency bifurcation of a flame in response to jet dynamics modulated by a transverse acoustic field

Florian LESPINASSE, Françoise BAILLOT
CORIA UMR 6614 CNRS, Site du Madrillet, 76801 Saint-Etienne-du-Rouvray, France

1   Introduction

Gas turbine regulations have led to the development of new combustion systems, but unfortunately these systems cause thermoacoustic instabilities [1]. In annular chambers, such instabilities are often driven by azimuthal modes, which may induce losses in combustion efficiency, or even structural damages. More and more numerical studies are dedicated to these technical and scientific problems (e.g. [2]), but experimental works are still limited, in particular where physical phenomena are finely described [3,4]. Laboratory research is thus crucial for highlighting the basic physical mechanisms driven by azimuthal modes and their coupling with flames. In such a context, we have conducted original experimental studies to quantify the dynamics of a laminar inverted conical flame, called a V-flame, modulated by transverse acoustic excitations in [5, 6]. They have shown new behaviors, in particular a nonlinear frequency bifurcation of the flame response induced by a vortex pairing phenomenon, and dissymmetric evolutions of jet and flame dynamics. A fine description of jet vortex dynamics appeared necessary to emphasize the mechanisms involved. This is the aim of the present study. Some of the results obtained in [5, 6] and the present working domain, are first introduced to give the framework of our approach. The frequency bifurcation of the flame response is analyzed for a symmetric flame placed at a pressure antinode. Then, it is quantified outside this location when the flow and flame are dissymmetric.

2   Experimental set-up and diagnostics

The experimental set-up, described in [5, 6], is composed of an acoustic cavity, two driver units, placed in its two opposite vertical walls, and a cylindrical burner vertically fixed at its bottom (see Fig.1). The vertical plates can slide on rails to adjust the distance between them, and thus ensure resonance of the acoustic pressure field at the forcing frequency f_0. By sliding the plates together, the burner of $10\,\mathrm{mm}$ exit diameter can be placed at any position inside the acoustic field. A central rod of $3\,\mathrm{mm}$ diameter is vertically aligned with the burner's axis; its extremity stands out by $3.5\,\mathrm{mm}$ above the burner exit. The acoustic burner response shows a peak, f_H, around $130\,\mathrm{Hz}$, and a secondary peak around $1\,\mathrm{kHz}$, respectively interpreted as a Helmholtz resonator mode and a $3/4$ wave mode.

Premixed methane-air flames are stabilized on the rod tip. Bulk velocity U_{bulk} is 2.1 m/s and the equivalence ratio is 1. The laminar flow shows no vortices, neither in the outer shear layer between the jet and the surrounding air, nor in the inner shear layer due to the rod. The streamlines are classically deviated

outwards from the vertical direction by the presence of the flame. The flame remains symmetric without acoustics. The global flame dynamics is characterized by CH* emission, characteristic of the heat release rate (h.r.r.) in the present conditions [6].

The position of a point is specified by means of the cavity coordinate system (O_c, X, Y, Z) where O_c is the center of the horizontal bottom plate, (O_c, X) is the axis normal to the plates and (O_c, Z) is the ascending vertical axis (see Fig.1). Pressure amplitudes $P_{ac}^*(X, Y, Z)$, measured along an X-axis, parallel to the acoustic axis, show an antinode at $X = 0$ and two minima near $X = \pm L_c/4$. An example of such a profile is given in Fig.2. Thus, pressure fluctuations $P_{ac}(X, Y, Z, t)$ may be expressed, in the domain $-L_c/4 \leq X \leq L_c/4$, as: $P_{ac}^*(X, Y, Z) \cos(2\pi f_0 t)$ with $P_{ac}^*(X, Y, Z) = P_a \cos(k_X X) \cos(k_Y Y) \cos(k_Z Z)$ and $k_X = (2\pi)/L_c$. It is interpreted as a planar standing wave in the X-direction, corresponding to the 2nd transverse cavity mode (see also [7]). The amplitude of fluctuations $P_{ac}(X, Y, Z, t)$, measured close to the pressure antinode (PA) at ($X = 10$ mm, $Y = 10$ mm, $Z = Z_b + 10$ mm), is noted P_{ref}. The center of the burner exit section, O_b, is positioned at ($X_b, Y_b = 0, Z_b = 20$ mm). In the following, positions of a measured quantity are specified by the burner coordinate system ($O_b, x = X - X_b, y = Y, z = Z - Z_b$). Local pressure fluctuation amplitudes, measured close to the burner exit ($x = 10$ mm, $y = 10$ mm, $z = 10$ mm), are noted $P_{b.e.}$.
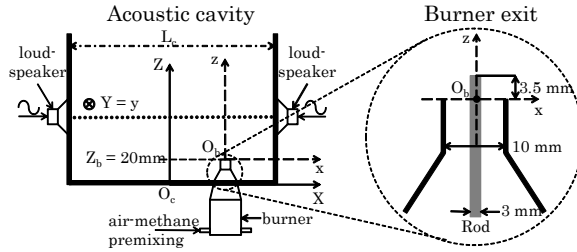

Figure 1: Sketch of the set-up. (O_c, X, Y, Z) coordinate system attached to cavity (solid line); (O_b, x, y, z) coordinate system attached to the burner (dashed line) ; acoustic axis at $Z = 92$mm (dotted line).
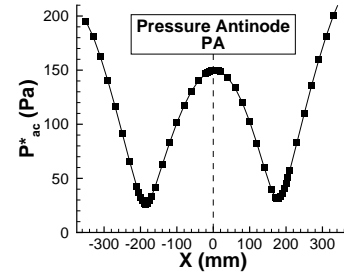
Figure 2: Experimental acoustic pressure amplitude field $|P_{ac}^*|$ vs. X for 510 Hz at ($X, Y = 0, Z = 30$mm) with $L_c = 75$ cm.

Several diagnostics are used to analyze how the flame and flow respond to a transverse wave. All measurements are made with a flame. A high-speed 2D scattering technique ($7\,920$ im./s) is used to visualize the flow structure by lighting the jet, seeded with oil droplets, by means of laser sheets created by a continuum laser. With this technique, the spatial flame evolution is followed over time in vertical laser sheets, containing both acoustic and burner axes, by following the droplet evaporation isotherm. Jet velocity data is measured by time-resolved Particle Image Velocimetry (PIV) (10^4 im./s). The flame dynamics is finally quantified by its overall CH* emission, recorded by a photomultiplier (PM) equipped with an interferential filter centered at $\lambda = 430$ nm with a FWHM $= 10$ nm (± 2 nm). Two microphones, one placed in the cavity and the other in the burner bottom, register pressure fluctuations.

3   Study background

In a previous study [6], a V-flame was positioned at different points of an acoustic transverse field. Original flame responses, localized in three spatial zones of the acoustic field, have been classified depending on the acoustic quantities involved in the process. They are: the velocity amplitude around the velocity antinode (VA) at $X = L_c/4$; the pressure amplitude around the pressure antinode PA at $X = 0$; and the pressure gradient between the two antinodes, which is maximum at the intensity antinode (IA) at $X = L_c/8$. Here, we focus on phenomena mainly driven by both the acoustic pressure and pressure gradient. The basin of influence widens from $-3/16\,L_c$ to $3/16\,L_c$ (see Fig.2).

As noted above, some results previously obtained in [5, 6] are first introduced. Concerning the pressure amplitude, it was quantified that its basic effect on the fluidic system was to modulate the mass flow rate at f_0 through the burner exit, in a similar way to what was observed by [4, 7]. Location PA was of particular interest, since the pressure amplitude was not influenced by any acoustic pressure gradient or velocity actions. There, analysis showed that the outer and inner shear layers, defined above, could be active. In the outer layer, the flow modulation induced vortices at the burner lip, formed at f_0. They were convected downstream until they impacted the flame and, for the low pressure amplitudes specified in [5], wrinkled it at f_0. This type of resulting flame is mentioned as a "wrinkled flame" in the following. For high pressure amplitudes, a pairing process occurred, but without any vortex merging before the vortices attained the front. It led to a subharmonic response of the flame dynamics with a rolling-up at $f_0/2$. The resulting flame is henceforth mentioned as a "rolled-up flame". Depending on frequency and pressure amplitude conditions (see [5]), the inner shear layer, produced behind the rod tip, could also yield a vortex shedding. Flame responses driven by the inner layer are not concerned here. The pressure amplitude also induced a vertical motion of the flame foot above the rod. For a sufficiently high pressure level, the flame blew out; the associated measured pressure amplitude is noted $P_{b.e.}^{bo}$ in the present work. Examples of its evolutions as a function of the burner location X_b are given in [6].

These behaviors were also noted in a wider spatial domain, marking out the basin of influence of PA (see [6]). However, they were conditioned by the influence of the pressure X-gradient, which imposed a response that was dissymmetric relative to the axial acoustic plane π for both flame and flow. Dissymmetry was quantified at the burner exit by the evolution of the two half-cross-section areas of the jet, measured on both sides of plane π, and also by phase-averaged median curves, indicating how the front deviated from its initial axisymmetry. Hereafter we focus on the fluidic mechanisms which lead to the subharmonic response of the "rolled-up flame" in the basin of PA. Results at $f_0 = 510\,\text{Hz}$ serve as an illustration, for which P_{ref} is not necessarily maintained constant in all the cases.

4   Subharmonic response at a pressure antinode

The present study completes results presented in [6]. In the illustrating examples at $f_0 = 510\,\text{Hz}$, $P_{b.e.}^{bo} = P_{ref} \approx 200\,\text{Pa}$. Flame dynamics is first characterized by its time front deformation. The evolution of local front undulations at a point G_i is quantified by applying a specific image processing to time-resolved series of tomography views; i are image line numbers. For that purpose, an adequate procedure (see similar approach in [6]) positions small interrogation windows in the vicinity of the contour determined by the evaporation isotherm on either side of the burner axis; the gray level, $I(t, G_i)$, in each window is then extracted and processed to obtain its frequency signature (e.g. in Fig.3). Flame dynamics is also described by the signal delivered by the overall CH* fluctuations, as mentioned above. The flow structure is also detailed to recognize and understand the main mechanisms leading to the various flame responses. Thus, tomography views, such as those reported in Fig.4, are used to characterize the outer shear-layer vortex morphology and topology. Vortex aspect is quantified by the local eccentricity $\epsilon_l = (a_M - a_m)/(a_M + a_m)$ with a_M and a_m the longest and the shortest vortex radii respectively. ϵ_l indicates the deformation intensity of a vortical structure from a circular shape ($\epsilon_l = 0$) to an ellipse flattened to a segment ($\epsilon_l \approx 1$). ϵ_l can be linked to the competition between the strain rate and the rotation rate which affect the structure. From now on, ϵ_l represents phase-averaged values of the eccentricity of an image series. To complete the vortex description, jet velocity fields are measured by time-resolved PIV from which vorticity fields are calculated. Phase-averaged velocities and vorticities from which vortex centers are determined, are presented in Fig.5. The paths of the centers, measured from the burner exit to the flame, are also reported in Fig.5, in which the values of the associated vorticities are noted by color levels. In the vortex initiation zone, as the vortices form at the burner exit, they adapt a circular

shape ($\epsilon_l \approx 0.03$). Then, they are ejected laterally before being pushed back towards the jet axis. In the convection zone, they move downstream towards the flame (see Fig.5).

(a) PA, $P_{b.e.} \approx 50\% P_{b.e.}^{bo}$.   (b) PA, $P_{b.e.} \approx 100\% P_{b.e.}^{bo}$.   (c) IA, $P_{b.e.} \approx 80\% P_{b.e.}^{bo}$.   (d) IA, $P_{b.e.} \approx 80\% P_{b.e.}^{bo}$.
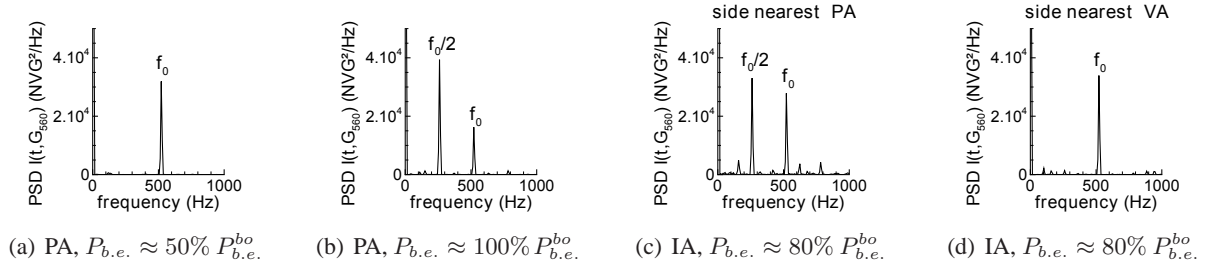
Figure 3: PSDs of $I(t, G_{560})$ from time-resolved series of tomography views; $P_{b.e.}^{bo}$ is: 200Pa for (a)-(b) and 250Pa for (c)-(d)

At low $P_{b.e.}(\approx 50\% P_{b.e.}^{bo})$, PSDs of $I(t, G_i)$, as shown in Fig.3(a), indicate that axisymmetric wrinkles are created at f_0. The front perturbation is also noted on the PSDs of the CH* fluctuations (see Fig.4(a)), and consequently the h.r.r. is modulated at f_0. Vortices are convected inside the flow, still little-modified compared to the no-forcing case. So vortex paths follow streamlines deviated towards the air, in a similar way to what is noted in a no-forcing flow with a V-flame (Fig.5(a)). They remain circular all along their displacement, but gradually lose their vorticity until they impact the flame and wrinkle the front at f_0.

(a) PA, $P_{b.e.} \approx 50\% P_{b.e.}^{bo}$.   (b) PA, $P_{b.e.} \approx 100\% P_{b.e.}^{bo}$.   (c) IA, $P_{b.e.} \approx 80\% P_{b.e.}^{bo}$.
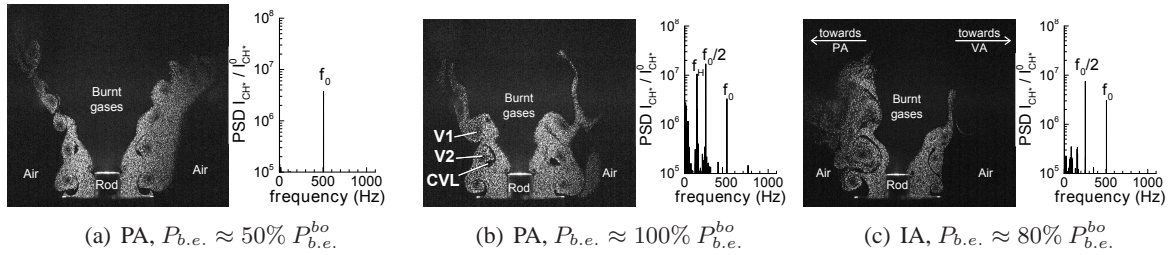
Figure 4: Vertical views of the seeded jet and PSD of CH* emission signals associated to each series; V1, V2: vortices; CVL: counter-rotating vortex layer; $P_{b.e.}^{bo}$ is: 200Pa for (a)-(b) and 250Pa for (c).

When $P_{b.e.}$ reaches 60%-$70\% P_{b.e.}^{bo}$, the front is still axisymmetric, but a large rolling-up occurs at its upper part. The rolling-up evolution, followed by $I(t, G_i)$, is modulated at $f_0/2$ (e.g. in Fig.3(b)). It leads to a strong fluctuation in the flame area over time at $f_0/2$ and can explain why the h.r.r. mainly fluctuates at $f_0/2$ too (see in Fig.4(b)). This is accompanied by a modification in the vortex evolution, although vortices are still produced at f_0. While the paths and the vorticity values of two successive vortices, labeled V1 and V2 for convenience, are almost similar in the initiation zone (see Fig.5(b)), in the convection zone they behave differently. This generates a pairing process which does not lead to merging in most cases. Indeed, after being formed, V1 remains circular during its downstream displacement (ϵ_l=0.08 at the flame impact zone, z=12 mm), as it is pushed towards the jet axis. It impacts the flame at its middle rather than at its extremity, as it does when $P_{b.e.}$ is low. Though its vorticity diminishes very little, its value is high enough to roll up the front (e.g. in Fig.5(b), $\Omega \approx 3500s^{-1}$ at the flame impact zone). The next vortex, V2, is much less deviated towards the jet axis than V1, increasing its distance to attain the flame. It is strongly stretched along its path such that its rotation practically stops (ϵ_l=0.56 at z=6 mm). Though the V2 path is also vertical, it has lost its vortical properties before reaching the flame ($\Omega \approx 0$ for y above location NV in Fig.5(b)). Its action on the flame is almost negligible.

Analyzing why V1 and V2 evolve differently is crucial to understanding the pairing mechanism. The above quantification of vortices implicitly considers that dynamics of a structure does not depend on

that of the others. It is insufficient. Indeed, multi-vortex quantities must be taken into account. For a f_0 flame response, the distance between two successive vortices first slightly increases before being almost constant until they impact the flame. The jet stretching produces streamwise filaments [8]. When a vortex forms, it engulfs some air, leading to the creation of a counter-rotating vorticity layer (CVL) (see Figs.4). At low $P_{b.e.}$, CVL rapidly loses its vorticity; its effect on the vortex is almost negligible. When the pairing process is set up, the distance between V1 and the downstream vortex V2 is lower than the distance with the upstream vortex V2. The two distances increase in a similar manner during vortex convection. This feature cannot explain satisfactorily why vorticity evolves differently for V1 and V2. When $P_{b.e.}$ increases sufficiently, CVLs modified by filaments have a significant action on V2. While the distances between V1 and CVLs increase during the vortex transport, CVLs approach V2, disturb it and finally lead to its destruction via vortex interactions. Distances between a vortex and CVLs are given in Fig.5(d). It is now clear why the flame is able to respond in a differentiated manner to V1 and V2, and consequently to have dynamics driven by the first sub-harmonic of the forcing frequency.
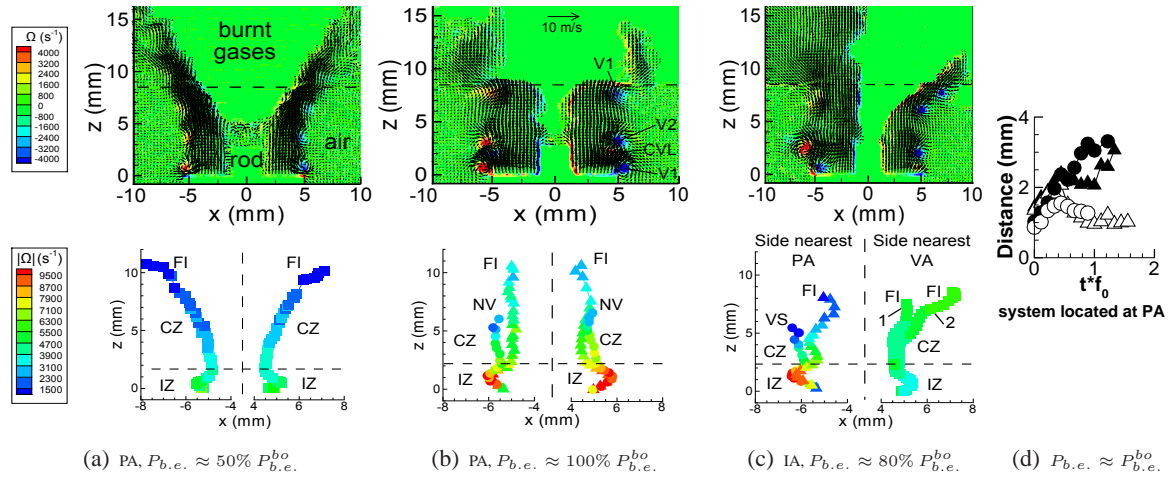

(a) PA, $P_{b.e.} \approx 50\% P_{b.e.}^{bo}$.   (b) PA, $P_{b.e.} \approx 100\% P_{b.e.}^{bo}$.   (c) IA, $P_{b.e.} \approx 80\% P_{b.e.}^{bo}$.   (d) $P_{b.e.} \approx P_{b.e.}^{bo}$.

Figure 5: **(a)-(c)** Two phase-averaged PIV fields joined at z=8.5 mm and vortex paths associated to each series for a duration $2/f_0$; IZ: initiation zone; CZ: convection zone; NV: no further vorticity; FI: flame impact. $\Delta t = 219\mu s$ between two following data; in (b-c): $\triangle$ V1, $\circ$ V2; in (c): 1 - vortex emitted with V1; 2 - vortex emitted with V2; $P_{b.e.}^{bo}$ is: 200Pa for (a), (b) and (d), and 250Pa for (c). **(d)** distances: ▲ V1/upstream CVL; ● V1/downstream CVL; $\triangle$ V2/upstream CVL; $\circ$ V2/downstream CVL.

5 Coupling between dissymmetry and the pairing process outside the pressure antinode

As noted above when the fluidic system is no longer located at PA, symmetry rupture of both flame and jet morphologies in the acoustic direction occurs [6]. It is marked by a discrepancy in the vortex formation/development and flame shape (wrinkling and tilting) between the regions located on both sides of the local axial plane π. Flow disturbances, and consequently flame undulations, are always maximum on the side nearer to PA (see Fig.4(c)). The pressure X-gradient is a necessary condition for dissymmetry. But in order that dissymmetry can be noted, a high enough pressure amplitude must also exist locally. Spatial dissymmetry distribution along the acoustic axis follows well that of the product of the amplitudes of the acoustic pressure X-gradient and the acoustic pressure. Below, illustrating measurements are given at IA where dissymmetry is important; there $P_{b.e.}^{bo}$ is 250 Pa with $P_{ref} = 380 Pa$.

At low $P_{b.e.}$ (50%-70% $P_{b.e.}^{bo}$), the two parts of the dissymmetric flame relative to plane π evolve at f_0. But for $P_{b.e.} \geq 70\% P_{b.e.}^{bo}$, a dissymetry in frequency response is added to dissymetric morphology. PSDs of $I(t, G_{i=560})$ given in Fig.3(c) show that the front located on the side nearest PA is modulated

at $f_0/2$, while in Fig.3(d) the front located on the side nearest VA is modulated at f_0. The flame area variation due to the $f_0/2$ modulation is larger than that due to the f_0 modulation, since it involves a strong rolling-up instead of a simple wrinkling. So, the h.r.r. mainly fluctuates at $f_0/2$ (see Fig.4(c)).

This difference of flame dynamics is induced by the flow itself. Where the pressure amplitude is the highest (side nearest PA), a vortex pair (V1, V2) can be produced, leading to a pairing process without merging, like that noted at PA (see Fig.5(c)). Where the pressure amplitude is the smallest (side nearest VA), the vortex pairing pattern is not totally established. Thus, two successive vortices still have similar features (see Fig.5(c)). Along their paths, they keep an almost constant vorticity, half of the maximum vorticity of V1 and V2 measured in their initiation zone (side nearest PA). It is consistent with the non persistence of CVLs, noted over time at IA (side nearest VA). But, their trajectories come to differ. This vortex array (side nearest VA) is an intermediate pattern between the ones leading to the "wrinkled flame" and the "rolled-up flame". Thus jet dynamics is split in two behaviors generated on either side of plane π, as vortices emitted from the burner exit are convected towards the flame.

6   Conclusion

This work details the subharmonic frequency bifurcation of a flame in a transverse acoustic field, by finely analyzing jet dynamics described by a vortex pairing process. Simultaneously, parts of the flame may respond at f_0 and $f_0/2$. This pairing, robust in the whole basin of influence of the pressure antinode, is conditioned by a dissymmetry imposed on both flame and flow by the pressure gradient. Moreover, as this pattern would be reproduced for any flame placed in the basin of PA, except at PA, the two parts of flames positioned side by side along the acoustic axis would be modulated at f_0 and $f_0/2$. This would create alternating pieces of flames modulated at f_0 and $f_0/2$. In combustion chambers, such flame dynamics suggests the occurrence of sudden jumps in thermo-acoustic instabilities, as noted in practice.

References

[1] F.E.C. Culick. (2006). Unsteady motions in combustion chambers for propulsion systems. RTO/NATO (Research and technology organisation) AGARDograph AG-AVT-039.

[2] P. Wolf et al. (2012). Acoustic and Large Eddy Simulation studies of azimuthal modes in annular combustion chambers. Combust. Flame. 159:3398.

[3] M. Hauser, M. Lorenz, T. Sattelmayer. (2010). Influence of transversal acoustic excitation of the burner approach flow on the flame structure, GT2010-22965 ASME.

[4] J. O'Connor, T. Lieuwen. (2011). Disturbance field characteristics of a transversely excited burner. Combust. Sci. Technol. 183(5):427.

[5] F. Lespinasse, F. Baillot, E. Domingues. (2011). Responses of laminar premixed flames to a high frequency transverse acoustic field. 5th Eur. Combust. Meet., Cardiff (UK).

[6] F. Lespinasse, F. Baillot, T. Boushaki. (2013). Responses of V-flames placed in an HF transverse acoustic field from a velocity to pressure antinode. C.R. Mecanique. 341.

[7] F. Baillot et al. (2009). On the behavior of an air-assisted jet submitted to a transverse high-frequency acoustic field. J. Fluid Mech. 640:305.

[8] D. Demare, F. Baillot. (2001). The role of secondary instabilities in the stabilization of a non-premixed lifted jet flame. Phys. Fluids. 13.